FEM-Based 3-D Tumor Growth Prediction for Kidney Tumor

Xinjian Chen, Ronald Summers, and Jianhua Yao*

Abstract—It is important to predict the tumor growth so that appropriate treatment can be planned in the early stage. In this letter, we propose a finite-element method (FEM)-based 3-D tumor growth prediction system using longitudinal kidney tumor images. To the best of our knowledge, this is the first kidney tumor growth prediction system. The kidney tissues are classified into three types: renal cortex, renal medulla, and renal pelvis. The reaction–diffusion model is applied as the tumor growth model. Different diffusion properties are considered in the model: the diffusion for renal medulla is considered as anisotropic, while those of renal cortex and renal pelvis are considered as isotropic. The FEM is employed to solve the diffusion model. The model parameters are estimated by the optimization of an objective function of overlap accuracy using a hybrid optimization parallel search package. The proposed method was tested on two longitudinal studies with seven time points on five tumors. The average true positive volume fraction and false positive volume fraction on all tumors is 91.4% and 4.0%, respectively. The experimental results showed the feasibility and efficacy of the proposed method.

Index Terms—Finite-element method (FEM), kidney tumor, segmentation, tumor growth prediction.

I. INTRODUCTION

KIDNEY cancer is among the ten most common cancers in both men and women. Overall, the lifetime risk for developing kidney cancer is about 1 in 75 (1.34%) [1]. It is important to predict the kidney tumor growth rate in clinical research so that appropriate treatment can be planned.

During the last three decades, the methods for simulating tumor growth have been extensively studied. Representative methods include mathematical models [2], [3], [19], cellular automata [4], finite element [3], [5], [19], and angiogenesis-based methods [6]. Swanson *et al.* [2] proposed to use the reaction–diffusion model to prediction the tumor growth in order to enhance the reality of medical imaging and highlight the inadequacies of current therapy. Clatz *et al.* [3] and Hoge *et al.* [19] improved this model by coupling diffusion model with biomechanical deformation. The techniques were applied to simulate the 3-D growth of brain tumors in MRIs. Mallet and Pillis [4] presented a model using cellular automata and partial differ-

ential equations (PDEs) to describe the interactions between a growing tumor next to a nutrient source and the immune system of the host organism. Mohamed and Davatzikos [5] present a 3-D mechanical model for simulating large nonlinear deformations induced by brain tumors to the surrounding encephalic tissues using the finite-element method (FEM). Tumor-induced angiogenesis has been modeled by many researchers. Lloyd *et al.* [6] presented a model of solid tumor growth, which can account for several stages of tumorigenesis. Plank *et al.* [24] proposed a nonlattice model to simulate sprouting angiogenesis. However, most of these methods are focused on brain tumor growth prediction. Only a few can be found for organs in the body region. Pathmanathan *et al.* [7] proposed to use the FEM and nonlinear elasticity to build a 3-D patient specific breast model. However, this method was not for tumor growth prediction. Instead, it was used to predict the tumor location.

The growth rate of renal tumors can be very slow. Kassouf *et al.* [9] followed up 24 patients over a period of average 24 months, and found noticeable tumor growth in only 5 patients during the surveillance period. Since the growth is slow, longitudinal studies over a long period of time are required to monitor the disease progress. A tumor growth prediction based on longitudinal studies over a short time period can help the physicians to plan the treatment in the early stage.

In this letter, we propose a tumor growth prediction system for kidney tumor based on FEM. The reaction–diffusion model is applied to model the kidney tumor growth and the FEM is used to simulate the diffusion process. The kidney tissues are classified into three main types: renal cortex, renal medulla, and renal pelvis (or collecting system). Based on [8] and [14], different diffusion properties are assigned to different kidney tissues: the renal cortex and renal pelvis are considered to be isotropic, while renal medulla to be anisotropic. The estimation of the tumor growth model parameters is essential for the tumor growth prediction. Clatz *et al.* [3] computed the brain tumor diffusion coefficients using the diffusion tensor image based on the assumption that the anisotropic ratio of diffusion is the same for water molecules and tumor cells. However, further experiments are needed to validate this hypothesis. In this letter, we propose an automated estimation of the model parameters via optimization of an objective function reflecting the overlap accuracy, which is executed in parallel using hybrid optimization parallel search (HOPSPACK) [22].

II. FEM-BASED TUMOR GROWTH PREDICTION

A. Overview of the Proposed Approach

The proposed tumor growth prediction system consists of three main phases: training, prediction, and validation. The

X. Chen and R. Summers are with the Department of Radiology and Imaging Sciences, National Institute of Health, Bethesda, MD 20892 USA (e-mail: chenx6@mail.nih.gov, rsummers@mail.nih.gov).

*J. Yao is with the Department of Radiology and Imaging Sciences, National Institute of Health, Bethesda, MD 20892 USA (e-mail: jyao@mail.nih.gov).
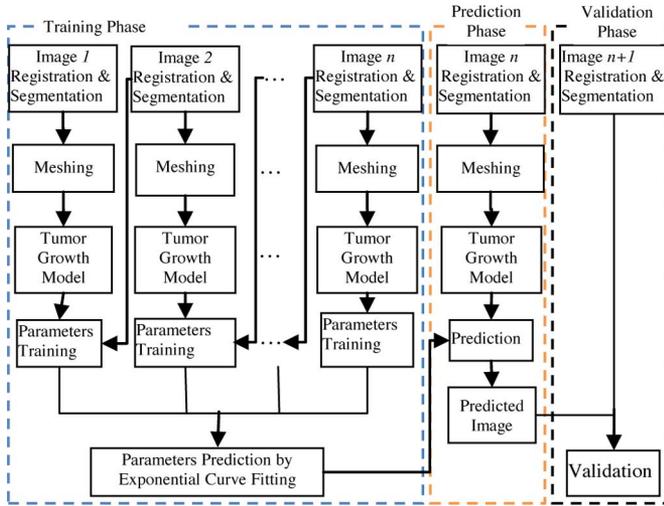
Fig. 1.   Flowchart of the proposed tumor growth prediction system.

flowchart is shown in Fig. 1. Suppose the longitudinal study has $n + 1$ time points. For the purpose of validation, we use first n time-point images for training, predict the tumor status at the $n + 1$th time point, and validate with the $n + 1$th images. In clinical practice, all $n + 1$ images are used to train the model parameters and predict the tumor status at a future time point. The training phase is composed of five steps. First, image registration and segmentation are conducted on the kidney images. Second, tetrahedral meshes are constructed for the segmented kidney and tumors, respectively. Third, the reaction–diffusion model is applied as the tumor growth model, and FEM is used to solve this PDE. Fourth, the parameters of the tumor growth model are optimized by HOPSPACK. Fifth, after computing the parameters based on the first n image, the model parameters for prediction at the $n + 1$th time point are estimated by an exponential curve fitting based on the nonlinear least-squares method. In the prediction phase, the estimated growth parameters are applied to the tumor growth model to compute the predicted result for time point $n + 1$ using image at time point n. In the validation phase, the predicted result is validated by comparing with image $n + 1$.

B. Registration and Image Segmentation

The baseline study is used as the reference study, and all other studies are registered to it via a rigid transformation. Then, the kidney is segmented by a graph-cut-oriented active appearance method (GC-OAAM) [10]. This method synergistically combines the active appearance, live-wire, and GC methods to take advantage of their complementary strengths. The details can be seen in [10]. After the kidney is segmented, the tumors, renal cortex, and renal pelvis are manually segmented, and the remaining tissues are treated as renal medulla.

C. Meshing

A tetrahedral mesh is built for the segmented tissues. The full meshing procedure is composed of the following three steps.

TABLE I
DIFFUSION PROPERTIES (D) OF DIFFERENT KIDNEY TISSUES

Tissue	Diffusivity
Renal cortex	D_c (isotropic)
Renal medulla	D_m (anisotropic): $D_{radical\ dir} = \lambda \cdot D_{other\ dirs}$
Renal pelvis	D_p (isotropic)

1) A surface mesh is first generated for the segmented tissues (kidney and tumors) by the marching cube algorithm [11].
2) This surface mesh is then decimated by the ISO2Mesh method [12].
3) The volumetric mesh is finally generated from the surface mesh also by the ISO2Mesh method [12].

D. Tumor Growth Model

The reaction–diffusion model is adopted to model the growth and spreading of tumor cells in the kidney. The reaction–diffusion model [3] was first proposed in chemistry, and widely used in biology, geology, physics, and ecology. The model is defined as follows:

$$\frac{\partial c}{\partial t} = -\mathrm{div}(-D\nabla c) + S(c, t) - T(c, t) \qquad (1)$$

where c represents the tumor cell density, D is the diffusion coefficient of tumor cells, $S(c, t)$ represents the source factor function that describes the proliferation of tumor cells, and $T(c, t)$ is used to model the efficacy of the tumor treatment.

Since our purpose is to predict the tumor growth before treatment, the treatment term $T(c, t)$ is omitted. The source factor $S(c, t)$ can be modeled using Gompertz law [3], which is defined as follows:

$$S(c, t) = \rho c \ln(\frac{C_{\max}}{c}) \qquad (2)$$

where ρ is the proliferation rate of tumor cells, $C_{\max}$ is the maximum tumor cell carrying capacity of the kidney tissue. Similar with [3], $C_{\max}$ is set to 3.5×10^4 cells mm^{-3}.

Combining (2) and (1) and omitting $T(c, t)$, we can get

$$\frac{\partial c}{\partial t} = -\mathrm{div}(-D\nabla c) + \rho c \ln\left(\frac{C_{\max}}{c}\right). \qquad (3)$$

Based on [8] and [14], in this letter, the diffusion in the renal cortex and renal pelvis are considered to be isotropic, while that in renal medulla to be anisotropic. The diffusion properties of different tissues are listed in Table I. It is important to note that in the diffusivity matrix D_m of medulla, the diffusion in the radial direction is faster than other directions. Here, the diffusivity in the radial direction is set as $\lambda (\lambda > 1)$ times than of those in other directions.

The FEM is used to solve the PDE in the aforementioned reaction–diffusion model. Based on the Galerkin method [15], the continuous problem can be converted to a discrete problem in a subvectorial space of finite dimension. In principle, it is the equivalent of applying the method of variation to a function space, by converting the equation to a weak formulation [15].

The details of implementation of the reaction–diffusion model by FEM can be found in [15].

E. Tumor Growth Model Parameters Training

In our tumor growth model, D_c, D_m, D_p, and ρ are the parameters that need to be estimated. The optimal set of tumor growth parameters for a particular patient is not known; it must be estimated from the patient's image. The optimizing of the tumor model parameters is based on the hypothesis that the optimal tumor parameters minimize the discrepancies between the simulated tumor image and the patient tumor image. It is achieved by solving the following optimization problem:

$$\theta^* = \arg\min_{\theta} E(\theta) \qquad (4)$$

where $\theta = \{D_c, D_m, D_p, \rho\}$, and E is the objective function. Many criteria can be used in constructing function E, such as the overlap accuracy, feature-based similarity, and smoothness of the registration [18]. Here, we only use the overlap accuracy. In this letter, we assumed that the diffusion properties for the tissues are not changed over the time, while the proliferation rate ρ could be changed. Suppose $\rho_1, \rho_2, \ldots, \rho_{n-1}$ are the proliferation rates corresponding to time points $t_1, t_2, \ldots, t_{n-1}$, respectively. Then, the parameters need to be estimated become exactly as: $\theta = \{D_c, D_m, D_p, \rho_1, \rho_2, \ldots, \rho_{n-1}\}$. As mentioned earlier, the first n studies are used for model parameters training. The parameters are trained in pair using consecutive study i and $I + 1$. Finally, our objective function is defined as follows:

$$E(\theta) = \sum_{i=1}^{n-1} w \cdot (1 - \text{TPVF}(I_{i,\theta}, I_{i+1})) + (1 - w)$$
$$\times \text{FPVF}(I_{i,\theta}, I_{i+1}) \qquad (5)$$

where I_{i+1} is used as the validation tumor image, and $I_{i,\theta}$ is the predicted tumor image using θ based on image I_i. For giving parameters θ, we can compute the density based on the tumor growth model. The threshold method is applied to detect the tumor. Tracqui et al. [17] suggested an 8000-cell mm^{-3} threshold of detection for an enhanced CT scan. This value is also applied in this letter. w is the weight for true positive volume fraction (*TPVF*) (in this letter $w = 0.5$). TPVF indicates the fraction of the total amount of tumor in the true prediction, and false positive volume fraction (FPVF) denotes the amount of tumor falsely identified; more details can be seen in [13].

The optimization of (5) is not a trivial task due to the discontinuities in the objective function. However, pattern search methods are suitable for such problems [22], [23]. They are directional methods that make use of a finite number of directions with appropriate descent properties. We apply HOPSPACK [22], which takes advantage of multithreading and parallel computing platforms. HOPSPACK comes with an asynchronous pattern search solver that handles general optimization problems with linear and nonlinear constraints, and continuous and integer-valued variables. Due to the complicated form of our objective function, it is not guaranteed that a global optimum exists. We set an iteration limit of 200 in the optimization process.
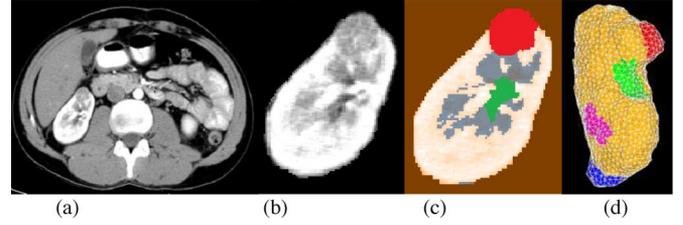

Fig. 2. Segmentation and meshing results for the first study. (a) Original image, (b) segmented kidney, (c) segmented tissues and one tumor (cortex: orange; medulla: black; pelvis: green; and tumor: red), and (d) one view of volumetric mesh (cortex: orange; pelvis: green; tumors: red; pink and blue, medulla is invisible because it is inside).

F. Tumor Growth Prediction

After getting the optimized parameters, these parameters are applied to the tumor growth model to compute the predicted result for time point $n + 1$ using image at time point n. For diffusion parameters, as we assume they will not change over the time, therefore, the optimized results are directly used. However, for the proliferation rate ρ, it will be changed over the time. Then, we need to predict the proliferation rate ρ for time point n based on the previously optimized $\rho_1, \rho_2, \ldots, \rho_{n-1}$. West et al. [20] shows that, regardless of the different masses and development times, mammals, birds, fishes, and mollusks, all share a common exponential tumor growth pattern. In this letter, we also assume the tumor growth follows this exponential law, which is defined as follows:

$$\rho = a * \exp(b * t) + c * \exp(d * t) \qquad (6)$$

where, a, b, c, and d are the growth coefficients. The curve fitting based on the nonlinear least-squares method is used for computing the predicted ρ. The detail can be seen in [21].

III. EXPERIMENTAL RESULTS

We tested the proposed methods on two longitudinal studies of kidney tumors. The contrast enhanced computed tomography (CT) images in arterial phase were used. Both studies had seven time-point images scanned at regular intervals of about half year over three to four years. Three kidney tumors were monitored for study 1, and two were monitored for study 2. The CT images were acquired from GE LightSpeed QX scanner with the slice spacing vary from 1.00 to 5.00 mm and pixel size = vary from 0.70×0.70 to 0.78×0.78 mm^2. All images were segmented manually by an expert to generate the ground truth.

Figs. 2 and 3 show the segmentation results and meshes for both patients, respectively. A mesh consisting of 7217 nodes and 40996 tetrahedra was generated for the first study, and 6666 nodes and 37857 tetrahedra for the second study.

As both studies had seven time-point images, the training of tumor growth model parameters were done on their first six images. The trained diffusivities and ρ for each tumor are shown in Table II and Fig. 4, respectively. These values are consistent with [2] and [14]. The average training time is about 260 min using MATLAB programming running on an Intel Xeon E5440 workstation with quad cores 8 threads (2.83GHz),
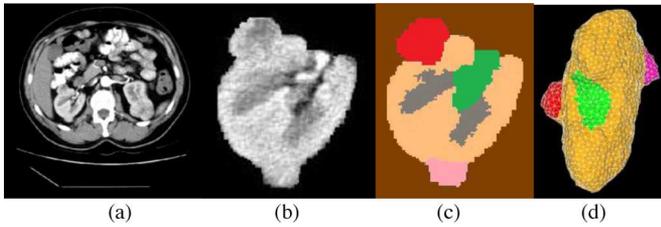
Fig. 3. Segmentation and meshing results for the second study. (a) Original image, (b) segmented kidney, (c) segmented tissues and two tumors (cortex: orange; medulla: black; pelvis: green; and tumors: red and pink), and (d) one view of volumetric mesh (cortex: orange; pelvis: green; tumors: red and pink).

TABLE II
TRAINED DIFFUSIVITIES FOR EACH TUMOR IN THE TWO STUDIES

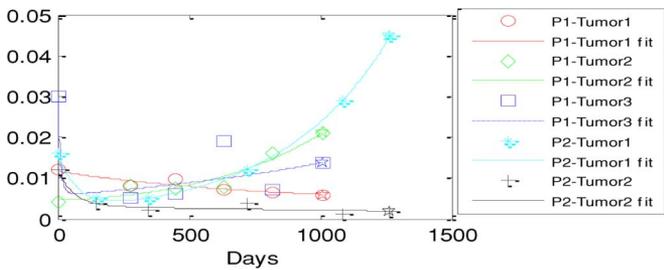| Diffusivity (mm^{-2}day^{-1})		Study #1			Study #2	
		Tumor1	Tumor2	Tumor3	Tumor1	Tumor2
D_c (isotropic)		0.084	0.089	0.098	0.085	0.068
D_m (anisotropic)	$D_{radical\ dir}$	0.075	0.081	0.088	0.076	0.059
	$D_{other\ dirs}$	0.063	0.067	0.075	0.065	0.051
	λ	1.190	1.209	1.173	1.169	1.157
D_p (isotropic)		0.096	0.102	0.112	0.098	0.078

Fig. 4. Parameter ρ curve fit by (6) for all five tumors. The fit was based on the five estimated values, the sixth value (overlap with ☆) was used for prediction also shown on the figure.

8 GB of RAM, which is currently done online. In the clinical application, this time is OK because the treatment planning or surgery decision is not required to make immediately after scanning, which is usually made after physicians' discussions based on many facts. However, this efficiency will be improved in the near future by including more training PCs and using C++ programming. The curve fitting based on (8) using nonlinear least-squares method was applied to these data. The computed ρ based on curve fit was applied on the sixth image to predict the tumor and validated with the seventh image. Figs. 5 and 6 show the predicted results for these two studies. We can find that the predicted results are quite good. As for prediction time, it is about 60 s.

As for quantitative evaluation, the TPVF and FPVF [13] are used to show the accuracy of the proposed method, and the results are also shown in Table III. The average TPVF and FPVF on all tumors are quite good, 91.4% and 4.0%, respectively. We also compared the volume difference result by our method with the Gompertz fit [3] method. In the 1960s, A. K. Laird [16] first successfully used the Gompertz curve to fit data of growth of tumors. The same training scheme was used, i.e., the Gompertz curve fit was based on the first six tumor volumes data, and
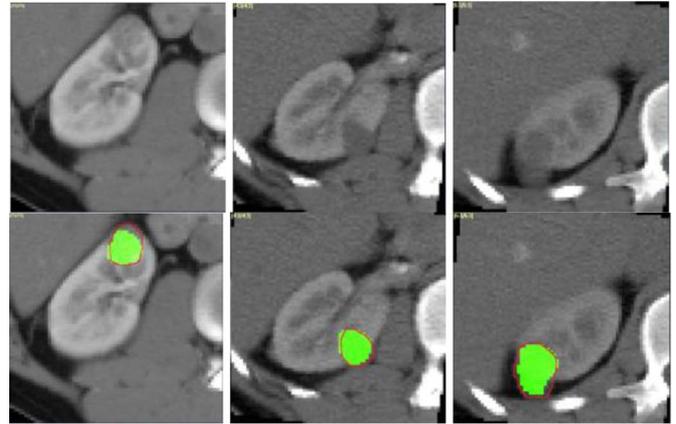

Fig. 5. Results of the tumor growth prediction on three slices for the first study. Top row shows the original images, and the bottom row shows the prediction results by green overlaid on the original images. Red lines represent the manually segmented tumor results. Different columns show different tumors.
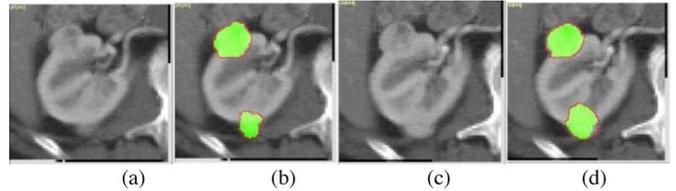

Fig. 6. Results of the tumor growth prediction on two slices for the second study. (a) and (c) are the original images. (b) and (d) show the prediction results by green overlaid on (a) and (c), respectively.

TABLE III
VOLUME DIFFERENCE, TPVF, AND FPVF FOR EACH TUMOR
IN THE TWO STUDIES

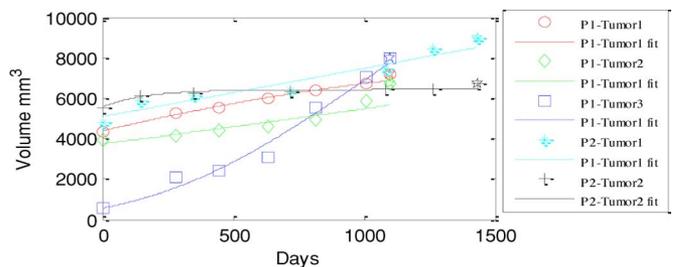|	Study #1			Study #2	
	Tumor1	Tumor2	Tumor3	Tumor1	Tumor2
Vol. diff. by Gompertz Fit	5.1%	17.1%	5.3%	5.5%	9.9%
Vol. diff. by our method	4.1%	5.1%	4.8%	4.5%	5.7%
TPVF	91.5%	90.9%	91.6%	92.1%	90.8%
FPVF	4.6%	4.2%	3.7%	3.5%	3.8%

Fig. 7. Tumor growth curve fit by Gompertz function for all five tumors. The fit was based on the first six volume data, and the seventh volume data (overlap with ☆) was also shown on the figure.

predicts the tumor volume for the seventh time point. The results for five tumors were show in Fig. 7 and Table III. Compared to Gompertz curve fit, our proposed method is more accurate.

IV. Perspectives and Future Work

In this letter, we adopted a widely used reaction–diffusion model as the tumor growth model. The proposed method was tested on two longitudinal studies with seven time points on five tumors. The preliminary experimental results proved the feasibility and efficacy of the proposed system. However, the mass effect was not taken into consideration. This will be done by coupling with biomechanical model in the near future as in [3] and [19]. Currently, we did not include the surrounding tissues as we found that the diffusion of the renal tumor is much faster in kidney than in the surrounding tissues. However, this is another important issue that will be investigated in our future work.

References

[1] American Cancer Society. (2010). [Online]. Available: http://www.cancer.org/docroot/cri/content/cri_2_4_1x_what_are_the_key_statistics_for_kidney_cancer_22.asp

[2] K. Swanson, C. Bridge, J. D. Murray, and E. C. Alvord, "Virtual and real brain tumors: Using mathematical modeling to quantify glioma growth and invasion," *J. Neurol. Sci.*, vol. 216, no. 1, pp. 1–10, Dec. 2003.

[3] O. Clatz, M. Sermesant, P.-Y. Bondiau, H. Delingette, S. K. Warfield, G. Malandain, and N. Ayache, "Realistic simulation of the 3-D growth of brain tumors in MR images coupling diffusion with biomechanical deformation," *IEEE Trans. Med. Imaging.*, vol. 24, no. 10, pp. 1334–1346, Oct. 2005.

[4] D. G. Mallet and L. G. D. Pillis, "A cellular automata model of tumor-immune interactions," *J. Theoretical Biol.*, vol. 239, no. 3, pp. 334–350, 2006.

[5] A. Mohamed and C. Davatzikos, "Finite element modeling of brain tumor mass-effect from 3D medical images," *Med. Image Comput. Comput.-Assisted Intervention (MICCAI '2005)*, vol. 3750, pp. 400–408.

[6] B. A. Lloyd, D. Szczerba, and G. Székely, "A coupled finite element model of tumor growth and vascularization," *Med. Image Comput. Comput.-Assisted Intervention (MICCAI '2007)*, pp. 874–881.

[7] P. Pathmanathan, D. J. Gavaghan, J. P. Whiteley, S. J. Chapman, and J. M. Brady, "Predicting tumor location by modeling the deformation of the breast," *IEEE Trans. Biomed. Eng.*, vol. 55, no. 10, pp. 2471–1480, Oct. 2008.

[8] H. Chandarana, E. Hecht, B. Taouli, and E. E. Sigmund, "Diffusion tensor imaging of *in vivo* human kidney at 3 T: Robust anisotropy measurement in the medulla," *Proc. Intl. Soc. Mag. Reson. Med.*, vol. 16, p. 494, 2008.

[9] W. Kassouf, A. G. Aprikian, M. Laplante, and S. Tanguay, "Natural history of renal masses followed expectantly," *J. Urol.*, vol. 171, pp. 111–113, 2004.

[10] X. Chen, J. Yao, Y. Zhuge, and U. Bagci, "3D automatic image segmentation based on graph cut-oriented active appearance models," *Int. Conf. Image Process. (ICIP)*, 2010, pp. 3653–3656.

[11] W. Lorensen and H. Cline, "Marching cubes: A high resolution 3-D surface construction algorithm," in *Proc. SIGGRAPH C. Graphics*, Jul. 1987, vol. 21, pp. 163–170.

[12] Q. Fang. *ISO2Mesh: A 3D surface and volumetric mesh generator for MATLAB/octave.* (2010). [Online]. Available: http://iso2mesh.sourceforge.net/cgi-bin/index.cgi?Home

[13] J. K. Udupa, V. R. Leblanc, Y. Zhuge, C. Imielinska, H. Schmidt, L. M. Currie, B. E. Hirsch, and J. Woodburn, "A framework for evaluating image segmentation algorithms," *Comput. Med. Imaging Graph.*, vol. 30, no. 2, pp. 75–87, 2006.

[14] M. Notohamiprodjo, C. Glaser, K. A. Herrmann, O. Dietrich, U. I. Attenberger, M. F. Reiser, S. O. Schoenberg, and H. J. Michaely, "Diffusion tensor imaging of the kidney with parallel imaging: Initial clinical experience," *Investigative Radiol.*, vol. 43, no. 10, pp. 677–685, Oct. 2008.

[15] A. l. Hanhart, M. K. Gobbert, and L. T. Izu, "A memory-efficient finite element method for systems of reaction-diffusion equations with non-smooth forcing," *J. Comp. Appl. Math.*, vol. 169, pp. 431–458, 2004.

[16] A. K. Laird, "Dynamics of tumor growth," *Brit. J. Cancer*, vol. 18, pp. 490–502, 1964.

[17] P. Tracqui, G. Cruywagen, D. Woodward, G. Bartoo, J. Murray, and E. Alvord, Jr., "A mathematical model of glioma growth: The effect of chemotherapy on spatio-temporal growth," *Cell Proliferation*, vol. 28, no. 1, pp. 17–31, Jan. 1995.

[18] E.I. Zacharaki, D. Shen, S. K. Lee, and C. Davatzikos, "ORBIT: A multiresolution framework for deformable registration of brain tumor images," *IEEE Trans. Med. Imag.*, vol. 27, no. 8, pp. 1003–1017, Aug. 2008.

[19] C. Hoge, C. Davatzikos, and G. Biros, "An image-driven parameter estimation problem for a reaction-diffusion glioma growth model with mass effects," *J. Math. Biol.*, vol. 56, pp. 793–825, 2008.

[20] G. B. West, J. H. Brown, and B. J. Enquist, "A general model for ontogenetic growth," *Nature*, vol. 413, pp. 628–631, 2001.

[21] C. T. Kelley, *Iterative Methods for Optimization.* Philadelphia, PA: SIAM, 1999.

[22] Todd D. Plantenga, "HOPSPACK 2.0 User Manual," Tech. Report SAND2009–6265, Sandia National Laboratories, Albuquerque, NM and Livermore, CA, Oct. 2009.

[23] G. A. Gray and T. G. Kolda, "Algorithm 856—APPSPACK 4.0: Asynchronous parallel pattern search for derivative-free optimization," *ACM Trans. Math. Softw*, vol. 32, pp. 485–507, 2006.

[24] M. J. Plank and B. D. Sleeman, "Lattice and non-lattice models of tumour angiogenesis," *Bull. Math. Biol.*, vol. 66, no. 6, pp. 1785–1819, 2004.